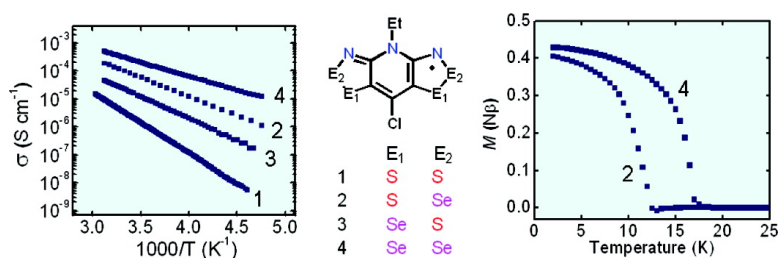


Enhanced Conductivity and Magnetic Ordering in Isostructural Heavy Atom Radicals

Craig M. Robertson, Alicea A. Leitch, Kristina Cvrkalj, Robert W. Reed, Daniel J. T. Myles, Paul A. Dube, and Richard T. Oakley

J. Am. Chem. Soc., **2008**, 130 (26), 8414-8425 • DOI: 10.1021/ja801070d • Publication Date (Web): 04 June 2008

Downloaded from <http://pubs.acs.org> on February 8, 2009



More About This Article

Additional resources and features associated with this article are available within the HTML version:

- Supporting Information
- Links to the 3 articles that cite this article, as of the time of this article download
- Access to high resolution figures
- Links to articles and content related to this article
- Copyright permission to reproduce figures and/or text from this article

[View the Full Text HTML](#)

Enhanced Conductivity and Magnetic Ordering in Isostructural Heavy Atom Radicals

Craig M. Robertson,[†] Alicea A. Leitch,[†] Kristina Cvrkalj,[†] Robert W. Reed,[†]
Daniel J. T. Myles,[†] Paul A. Dube,[‡] and Richard T. Oakley*[†]

Department of Chemistry, University of Waterloo, Waterloo, Ontario N2L 3G1, Canada, and
Brockhouse Institute for Materials Science, McMaster University, Hamilton,
Ontario L8S 4L8, Canada

Received February 19, 2008; E-mail: oakley@uwaterloo.ca

Abstract: Synthetic methods have been developed to generate the complete series of resonance-stabilized heterocyclic thia/selenazyl radicals **1a–4a**. X-ray crystallographic studies confirm that all four radicals are isostructural, belonging to the tetragonal space group $P4_21m$. The crystal structures consist of slipped π -stack arrays of undimerized radicals packed about $\bar{4}$ centers running along the z direction, an arrangement which gives rise to a complex lattice-wide network of close intermolecular $E_2\cdots E_2'$ contacts. Variable temperature conductivity (σ) measurements reveal an increase in conductivity with increasing selenium content, particularly so when selenium occupies the E_2 position, with $\sigma(300\text{ K})$ reaching a maximum (for $E_1 = E_2 = \text{Se}$) of $3.0 \times 10^{-4}\text{ S cm}^{-1}$. Thermal activation energies E_{act} follow a similar profile, decreasing with increasing selenium content along the series **1a** (0.43 eV), **3a** (0.31 eV), **2a** (0.27 eV), **4a** (0.19 eV). Variable temperature magnetic susceptibility measurements indicate that all four radicals exhibit $S = 1/2$ Curie–Weiss behavior over the temperature range 20–300 K. At lower temperatures, the three selenium-based radicals display magnetic ordering. Radical **3a**, with selenium positioned at the E_1 site, undergoes a phase transition at 14 K to a weakly spin-canted ($\phi = 0.010^\circ$) antiferromagnetic state. By contrast, radicals **2a** and **4a**, which both possess selenium in the E_2 position, order ferromagnetically, with Curie temperatures of $T_c = 12.8$ and 17.0 K, respectively. The coercive fields H_c at 2 K of **2a** (250 Oe) and **4a** (1370 Oe) are much larger than those seen in conventional light atom organic ferromagnets. The transport properties of the entire series **1a–4a** are discussed in the light of Extended Hückel Theory band structure calculations.

Introduction

For many years the pursuit of molecular materials exhibiting conductive properties has been based on the charge transfer (CT) paradigm, within which charge carriers are generated by CT between an electron donor and an electron acceptor.^{1,2} Typically, two separate components are employed for this purpose, although conductive materials that are nominally single component can be made by imbedding donor and acceptor moieties into the same molecule.³ The two-component approach has also

been adapted to allow the fabrication of materials that show both conductive and magnetic properties. In general, magnetically active (inorganic) anions are incorporated into a cation/anion framework in which the (organic) cations provide the charge carriers and the conduction pathway.⁴ These systems are of particular appeal as their multifunctional capability may lead to the development of molecular spintronic materials.⁵

To date there is little precedent for the idea of building single component molecular materials with both conductive and magnetic behavior,⁶ as the design criteria are demanding. The minimum requirement would be a molecule that possesses at least one unpaired electron capable of serving as both a charge carrier and magnetic coupler. In principle, this condition can be fulfilled by molecular radicals. Extensive work over the last

[†] University of Waterloo.

[‡] McMaster University.

- (1) (a) Garito, A. F.; Heeger, A. J. *Acc. Chem. Res.* **1974**, *7*, 232. (b) Torrance, J. B. *Acc. Chem. Res.* **1979**, *12*, 79. (c) Williams, J. M.; Ferraro, J. R.; Thorn, R. J.; Carlson, K. D.; Geiser, U.; Wang, H. H.; Kini, A. M.; Whangbo, M.-H. *Organic Superconductors (Including Fullerenes)*; Prentice Hall: Englewood Cliffs, 1992.
- (2) (a) Bendikov, M.; Wudl, F.; Perepichka, D. F. *Chem. Rev.* **2004**, *104*, 4891. (b) Jérôme, D. *Chem. Rev.* **2004**, *104*, 5565. (c) Geiser, U.; Schlueter, J. A. *Chem. Rev.* **2004**, *104*, 5203. (d) Yamada, J.; Akutsu, H.; Nishikawa, H.; Kikuchi, K. *Chem. Rev.* **2004**, *104*, 5057. (e) Saito, G.; Yoshida, Y. *Bull. Chem. Soc. Jpn.* **2007**, *80*, 1.
- (3) (a) Tanaka, H.; Okano, Y.; Kobayashi, H.; Suzuki, W.; Kobayashi, A. *Science* **2001**, *291*, 285. (b) Tanaka, H.; Tokumoto, M.; Ishibashi, S.; Graf, D.; Choi, E. S.; Brooks, J. S.; Yasuzuka, S.; Okano, Y.; Kobayashi, H.; Kobayashi, A. *J. Am. Chem. Soc.* **2004**, *126*, 10518. (c) Kobayashi, A.; Sasa, M.; Suzuki, W.; Fujiwara, E.; Tanaka, H.; Tokumoto, M.; Okano, Y.; Fujiwara, H.; Kobayashi, H. *J. Am. Chem. Soc.* **2004**, *126*, 426. (d) Kobayashi, A.; Fujiwara, E.; Kobayashi, H. *Chem. Rev.* **2004**, *104*, 5243.

- (4) (a) Coronado, E.; Galán-Mascarós, J. R.; Gómez-García, C. J.; Laukhin, V. *Nature* **2000**, *408*, 447. (b) Coronado, E.; Day, P. *Chem. Rev.* **2004**, *104*, 5419. (c) Coronado, E.; Giménez-Saiz, C.; Gómez-García, C. J. *Coord. Chem. Rev.* **2005**, *249*, 1776. (d) Coronado, E.; Galán-Mascarós, J. R. *J. Mater. Chem.* **2005**, *15*, 66.
- (5) (a) Wolf, S. A.; Awschalom, D. D.; Buhrman, R. A.; Daughton, J. M.; von Molnár, S.; Roukes, M. L.; Chtchelkanova, A. Y.; Trege, B. D. M. *Science* **2001**, *294*, 1488. (b) Prinz, G. A. *Science* **1998**, *282*, 1660. (c) Naber, W. J. M.; Faez, S.; van der Wiel, W. G. *J. Phys. D: Appl. Phys.* **2007**, *40*, R205.
- (6) Itkis, M. E.; Chi, X.; Cordes, A. W.; Haddon, R. C. *Science* **2002**, *296*, 1443.

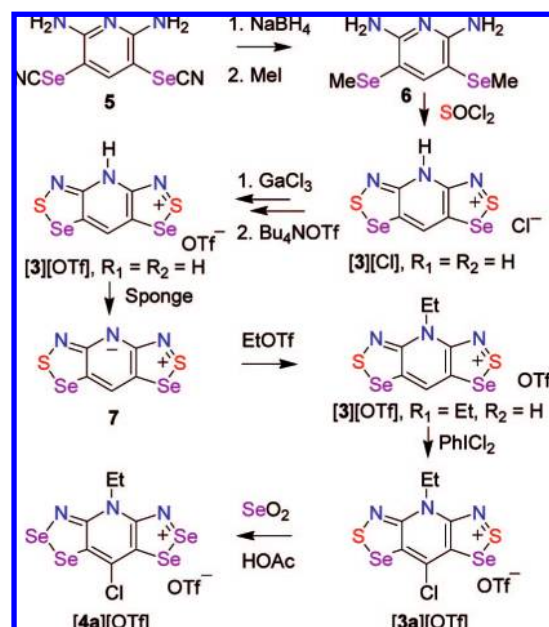
radicals,^{25,26} was a problem but one that could be overcome by judicious choice of ligands.²⁷ More recent work has afforded general synthetic routes to **3** and **4** and confirmed that (i) isostructural mapping was possible and (ii) replacement of sulfur by selenium did indeed lead to an improvement in conductivity.²⁸ What also emerged from these initial explorations was the realization that the presence of the heavy heteroatom could enhance not only charge transport but also magnetic exchange interactions. Radicals **3** and **4** ($R_1 = \text{Et}$, $R_2 = \text{H}$), for example, undergo magnetic ordering to spin-canted antiferromagnetic states at temperatures of 18 and 27 K, respectively,²⁹ while **2** ($R_1 = \text{Et}$, $R_2 = \text{Cl}$, hereafter termed **2a**, as in Chart 1) orders as a bulk ferromagnet with T_c near 12 K.³⁰

In this paper we build on our preliminary work on **2a**,³⁰ providing a full account of the synthesis, spectroscopic, electrochemical, and structural (at 100 and 295 K) characterization of the family of S/Se-based radicals **1a–4a**. These four compounds constitute a complete isostructural set, all belonging to the tetragonal space group $P4_2/m$. Variable temperature (AC and DC) magnetic susceptibility and four-probe conductivity measurements have been performed on the selenium-based radicals **2a**, **3a**, and **4a**. The results provide a pleasing and dramatic display of the effect of the placement (E_1 versus E_2) of selenium on transport properties. Conductivities increase and thermal activation energies decrease with selenium content along the series **1a**, **3a**, **2a**, **4a**, in accord with trends in bandwidth estimated from Extended Hückel Theory (EHT) band structure calculations. Magnetic exchange interactions also vary along the series. Thus, in contrast to the ferromagnet **2a** ($E_2 = \text{Se}$), radical **3a** ($E_1 = \text{Se}$) behaves as a spin-canted antiferromagnet, ordering near 14 K. Bulk ferromagnetic ordering returns in radical **4a**, and the Curie temperature increases to $T_c = 17$ K.

Results

Synthesis. Preparative routes to salts of the all-sulfur framework **1a**, using the double Herz cyclization of an *N*-alkylated diaminopyridinium salt with sulfur halides, are now well established.²⁰ Our initial approach for the generation of derivatives of **2a**, with selenium in the E_2 -position, was based on the condensation of *S*-acetylated pyridinedithiols with selenium halides, which provided an effective but somewhat lengthy preparative procedure.²⁴ More recently we have taken advantage of chemistry developed 30 years ago³¹ for the direct incorporation of selenium into the 2-position of monofunctional 1,2,3-

Scheme 1



dithiazolylum salts using SeO_2 .³² The method is readily applicable to the present bifunctional systems and allows for the direct conversion of $[\mathbf{1a}]^+$ into $[\mathbf{2a}]^+$ in a single step.^{27a}

The preparation of salts of $[\mathbf{3a}]^+$ and $[\mathbf{4a}]^+$, which possess selenium in the E_1 -position, required an *ab initio* approach (Scheme 1) starting from the diaminopyridine-bis(selenocyanate) **5**, reduction, and methylation of which readily afforded the corresponding bis(selenomethyl) derivative **6**. Methylation (rather than protonation) was necessary, as attempts to protonate the intermediate selenolate invariably produced an insoluble polymeric diselenide that would not undergo ring closure with sulfur halides. By contrast, reaction of **6** with thionyl chloride in the presence of triethylamine led to removal of the methyl groups and cyclocondensation to the desired framework in the form of the protonated salt $[\mathbf{3}][\text{Cl}]$ ($R_1 = R_2 = \text{H}$). Treatment of this crude material, a black insoluble powder, with gallium trichloride produced a soluble (in MeCN) tetrachlorogallate salt, which was metathesized with tetrabutylammonium triflate to generate the corresponding triflate. Deprotonation of this salt with Proton Sponge afforded the zwitterion **7**, and treatment of the latter compound with ethyl triflate in the presence of Proton Sponge yielded the *N*-ethyl triflate $[\mathbf{3}][\text{OTf}]$ ($R_1 = \text{Et}$, $R_2 = \text{H}$), which could be chlorinated with iodobenzene dichloride to give the desired salt $[\mathbf{3a}][\text{OTf}]$. Conversion of $[\mathbf{3a}][\text{OTf}]$ to $[\mathbf{4a}][\text{OTf}]$ utilized the SeO_2 insertion method described above. Like $[\mathbf{1a}][\text{OTf}]$, the triflate salts of $[\mathbf{2a}]^+$, $[\mathbf{3a}]^+$, and $[\mathbf{4a}]^+$ were easily crystallized from either MeCN or HOAc as deep red/purple needles. The resulting materials are indefinitely stable in air.

Reduction of the triflate salts of $[\mathbf{2a}]^+$, $[\mathbf{3a}]^+$, and $[\mathbf{4a}]^+$ to afford crystals of the corresponding radicals can be effected chemically and, in one case, electrochemically. We have explored a variety of chemical reducing agents, including deca-, octa- and hexamethylferrocene (DMFc, OMFc, and HMFc, respectively), tetrakisdimethylaminoethylene (TDAE), and *N,N,N',N'*-

- (25) (a) Cordes, A. W.; Haddon, R. C.; Oakley, R. T.; Schneemeyer, L. F.; Waszczak, J. V.; Young, K. M.; Zimmerman, N. M. *J. Am. Chem. Soc.* **1991**, *113*, 582. (b) Andrews, M. P. *J. Am. Chem. Soc.* **1991**, *113*, 3559. (c) Cordes, A. W.; Haddon, R. C.; Hicks, R. G.; Oakley, R. T.; Palstra, T. T. M.; Schneemeyer, L. F.; Waszczak, J. V. *J. Am. Chem. Soc.* **1992**, *114*, 1729.
- (26) (a) Feeder, N.; Less, R. J.; Rawson, J. M.; Oliete, P.; Palacio, F. *Chem. Commun.* **2000**, 2449. (b) Parvez, M.; Boeré, R. T. *Acta Crystallogr. C* **1995**, *51*, 2118.
- (27) (a) Brusso, J. L.; Derakhshan, S.; Itkis, M. E.; Kleinke, H.; Haddon, R. C.; Oakley, R. T.; Reed, R. W.; Richardson, J. F.; Robertson, C. M.; Thompson, L. K. *Inorg. Chem.* **2006**, *45*, 10958. (b) Beer, L.; Brusso, J. L.; Haddon, R. C.; Itkis, M. E.; Oakley, R. T.; Reed, R. W.; Richardson, J. F.; Secco, R. A.; Yu, X. *Chem. Commun.* **2005**, 5745.
- (28) Brusso, J. L.; Cvrkalj, K.; Leitch, A. A.; Oakley, R. T.; Reed, R. W.; Robertson, C. M. *J. Am. Chem. Soc.* **2006**, *128*, 15080.
- (29) Leitch, A. A.; Brusso, J. L.; Cvrkalj, K.; Reed, R. W.; Robertson, C. M.; Dube, P. A.; Oakley, R. T. *Chem. Commun.* **2007**, 3368.
- (30) Robertson, C. M.; Myles, D. J. T.; Leitch, A. A.; Reed, R. W.; Dooley, D. M.; Frank, N. L.; Dube, P. A.; Thompson, L. K.; Oakley, R. T. *J. Am. Chem. Soc.* **2007**, *129*, 12688.
- (31) Akulin, Y. I.; Gel'mont, M. M.; Strelets, B. Kh.; Efros, L. S. *Khim. Geterotsikl. Soedin.* **1978**, 912.

- (32) A similar approach has been used to incorporate selenium into dithiadiazolylum salts. For example, see: Less, R. J.; Rawson, J. M.; Jones, M. *Polyhedron* **2001**, *20*, 523.

Table 1. Hyperfine Coupling Constants, *g*-Values, and Half-Wave Potentials^a

	1a	2a	3a	4a
a_N (mT)	0.310 (2N) 0.060 (1N)	0.310 (2N) 0.060 (1N)	0.32 (2N) 0.05 (1N)	0.32 (2N) 0.05 (1N)
<i>g</i> -value	2.0082	2.0111	2.0190	2.0284
$E_{1/2}^{-1/0}$ (V)	-0.845	-0.731	-0.813	— ^c
$E_{1/2}^{0/+1}$ (V)	-0.018	0.013	0.026	0.053 ^d
$E_{1/2}^{+1/+2}$ (V)	1.390	1.343	1.311	1.267
E_{cell}^b (V)	0.827	0.744	0.839	—

^a $E_{1/2}$ values (V) in MeCN, ref SCE. ^b $E_{\text{cell}} = E_{1/2}^{0/+1} - E_{1/2}^{-1/0}$. ^c No wave observed. ^d Reversible wave at 45 °C and 1000 mV s⁻¹.

tetramethyl-*p*-phenylenediamine (TMPDA).³³ The eventual choice of reagent was dictated in part by the reduction potentials of the cations (vide infra) and partly by concerns about potential contamination of the resulting radicals by paramagnetic byproducts, notably ferrocenium salts. Thus, while OMFc performed admirably, and provided single crystals of **2a** and **3a** suitable for X-ray work, we moved to TDAE in order to eliminate the possibility of metal contamination of samples used for magnetic measurements. TDAE is, however, a more potent reductant, and while it provided analytically pure material, magnetic measurements (vide infra) indicated the production of small amounts of diamagnetic material, possibly dimers. Eventually, we turned to TMPDA, a much milder reagent which afforded clean, defect-free, microcrystalline material. The magnetic data reported in this work refer to samples of the radicals generated in this way. Crystals of **4a** of sufficient size for X-ray data collection could not be grown by chemical reduction. Satisfyingly, however, the conductivity of this material was such that high quality needles could be grown by electrocrystallization. This is, to our knowledge, the first instance where this technique has been applied to the growth of a neutral radical.

EPR Spectroscopy and Cyclic Voltammetry. Electron paramagnetic resonance (EPR) studies on **1a** provided confirmation of a highly delocalized spin distribution, the characteristic five-line hyperfine pattern arising from spin coupling to two equivalent ¹⁴N nuclei on the two dithiazolyl rings.²⁰ As expected, the observed a_N values (Table 1) are about one-half those seen in monofunctional dithiazolyls.³⁴ There are also smaller couplings to the central pyridine nitrogen which can be extracted by spectral simulation. The selenium-based radicals **2a–4a** are less soluble than **1a**, and solution-based spectra were more difficult to obtain. Good signal-to-noise ratios were eventually achieved by dissolving the radicals in hot degassed toluene. The X-band EPR spectra of the complete series **1a–4a** (recorded at ambient temperature) are shown in Figure 1. The same five-line appearance is seen in all cases, but the incorporation of selenium leads to a progressive line-broadening caused by spin-orbit coupling. For the same reason there is also a slight increase in the *g*-value (Table 1), but otherwise the similarity in the spectra confirm the same basic spin distribution, a conclusion predicted by theoretical calculations.^{24b}

The electrochemical behavior of **1a–4a** has been probed by cyclic voltammetry on solutions of the triflate salts [**1a–4a**][OTf] in MeCN (with 0.1 M *n*-Bu₄NPF₆ as supporting electrolyte). The results are presented in the form of half-wave

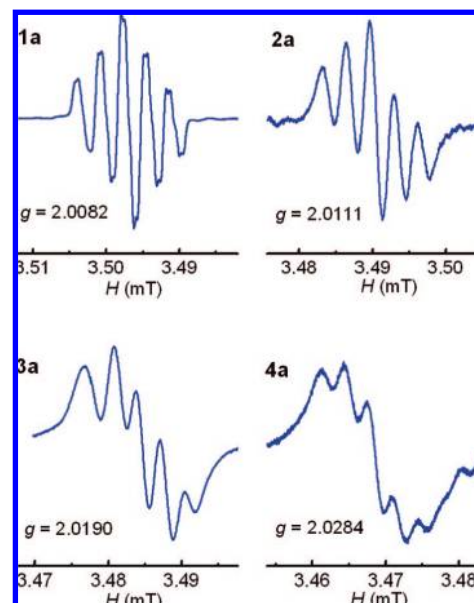


Figure 1. X-band EPR spectra of **1a–4a** in toluene, SW = 30 mT. Derived hyperfine coupling constants and *g*-values are listed in Table 1.

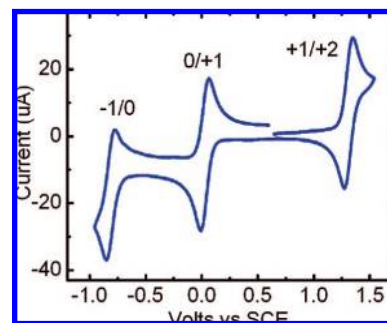


Figure 2. Cyclic voltammetry on [**3a**][OTf] in MeCN.

potentials $E_{1/2}$ in Table 1, and a representative scan (for **3a**) is illustrated in Figure 2. Compounds **1a**, **2a**, and **3a** all show three reversible waves, corresponding to the $-1/0$, $0/+1$, and $+1/+2$ processes. In the case of **4a**, the two more positive waves are reversible, but the $-1/0$ wave collapses completely as a result of deposition of the radical on the electrode. The $0/+1$ couple also becomes strongly irreversible if the scan range is taken to potentials significantly more cathodic than that of the $0/+1$ process. Although the E_{cell} data do not form a complete set (the $E_{1/2}^{-1/0}$ value for **4a** is not available), some observations can be made about electronic changes along the series **1a** to **4a**. First, there is a slight anodic shift in the $E_{1/2}^{0/+1}$ value with increasing selenium content. This change is in accord with the results of calculated (B3LYP/6-31G(d,p)) ionization potentials^{24b} but not sufficiently large to influence the choice of chemical reducing agent for the generation of the radicals. Likewise the slight decrease in cell potential E_{cell} between **1a** and **2a** parallels the changes in computed gas phase disproportionation energies on model structures^{24b} and augurs well for a slight decrease in the on-site Coulomb repulsion term *U* with increasing selenium content in the E₂ position.

Crystal Structures. Unit cell information and selected metrics on **1a–4a**, derived from X-ray data collected at ambient temperature, are presented in Table 2. We have also collected full data sets at 100 K, and structural summaries from these refinements are catalogued in the Supporting Information. The

(33) See the Supporting Information for a table of half-wave potentials of the reducing agents used in this work.

(34) (a) Cordes, A. W.; Mingie, J. R.; Oakley, R. T.; Reed, R. W.; Zhang, H. *Can. J. Chem.* **2001**, *79*, 1352. (b) Beer, L.; Cordes, A. W.; Haddon, R. C.; Itkis, M. E.; Oakley, R. T.; Reed, R. W.; Robertson, C. M. *Chem. Commun.* **2002**, 1872.

Table 2. Crystal Data and Metrics for 1a–4a

	1a ^a	2a ^b	3a	4a
formula	C ₇ H ₅ ClN ₃ S ₄	C ₇ H ₅ ClN ₃ S ₂ Se ₂	C ₇ H ₅ ClN ₃ S ₂ Se ₂	C ₇ H ₅ ClN ₃ Se ₄
<i>M</i>	294.83	388.63	388.63	482.43
<i>a</i> (Å)	15.886(4)	16.0334(8)	16.2708(5)	
<i>c</i> (Å)	4.1088(11)	4.1090(4)	4.1599(2)	4.1720(3)
<i>V</i> (Å ³)	1036.9(5)	1056.30(13)	1072.47(6)	1104.49(9)
ρ_{calcd} (g cm ⁻³)	1.889	2.444	2.407	2.901
space group	<i>P</i> 4 ₂ <i>m</i>	<i>P</i> 4 ₂ <i>m</i>	<i>P</i> 4 ₂ <i>m</i>	<i>P</i> 4 ₂ <i>m</i>
<i>Z</i>	4	4	4	4
temp (K)	293(2)	298(2)	295(2)	296(2)
μ (mm ⁻¹)	1.137	7.613	7.498	13.494
λ (Å)	0.71073	0.71073	0.71073	0.71073
data/restr./parameters	1064/0/87	1150/0/76	2150/0/76	1209/0/76
solution method	direct methods	direct methods	direct methods	direct methods
<i>R</i> , <i>R</i> _w (on <i>F</i> ²)	0.0279, 0.0571	0.0447, 0.1003	0.0402, 0.0822	0.0374, 0.0635
<i>E</i> ₁ – <i>E</i> ₂ (Å)	2.1049(12)	2.249(2)	2.2325(9)	2.3614(10)
<i>E</i> ₂ – <i>N</i> (Å)	1.663(3)	1.805(6)	1.660(3)	1.829(5)
<i>E</i> ₁ – <i>C</i> (Å)	1.728(3)	1.733(7)	1.863(3)	1.868(6)
<i>d</i> ₁ (Å)	3.401(1)	3.328(1)	3.439(2)	3.404(1)
<i>d</i> ₂ (Å)	3.560(1)	3.459(1)	3.588(2)	3.502(1)
<i>d</i> ₃ (Å)	3.573(1)	3.655(2)	3.467(1)	3.618(1)
δ (Å)	3.483(12)	3.516(7)	3.511(3)	3.545(6)
τ (deg)	57.9(3)	58.83(1)	57.57(1)	58.18(2)
deviation from plane (Å) ^c	0.0663	0.087	0.0790	0.0843

^a Data from ref 20a. ^b Data from ref 30. ^c Mean value of deviations of all atoms from plane of heterocyclic framework.

results establish that the four compounds are isostructural, all crystallizing in the tetragonal space group *P*4₂*m*. As we had desired, dimerization is suppressed across the entire series, even at low temperatures (100 K). At the molecular level the intramolecular distances and angles are typical for this class of heterocyclic radical, the internal *E*₁–*E*₂, *E*₂–*N*, and *E*₁–*C* bonds being slightly longer than in the corresponding cations. The difference can be ascribed to the antibonding nature of the radical SOMO, which is not occupied in the cation.²⁰

The crystal structures consist of undimerized radicals bisected by mirror planes which generate 4-fold pinwheel-like clusters about the 4 centers. The radicals pack in slipped π -stack arrays running along the *z*-direction. The mean interplanar separations δ and the inclination angle τ of the mean molecular plane with respect to the stacking axis are listed in Table 2.^{20c} Representative views of the packing of 4a, along directions parallel and perpendicular to the stacking axis, are shown in Figure 3. The radicals are not dimerized; that is, there is no pairing of spins into a localized covalent bond. There is, however, an extensive lattice-wide network of intermolecular interactions which lace the radicals together along the stacking direction and perpendicular to it in both the *x* and *y* directions. The *E*–*E'* contacts *d*₁–*d*₃ to/from a single radical are shown in Figure 4, using 4a as an example, along with the weblike patterns that these generate along and about the 4 centers. All these contacts are well within the nominal van der Waals separation for sulfur (3.6 Å) and selenium (3.8 Å).³⁵ Of particular note is the contraction in *d*₁ and *d*₂ in 2a and 4a relative to 1a and 3a, respectively (Figure 5).³⁶ The closer interactions found when selenium occupies the *E*₂ site are reminiscent of the contractions in intermolecular contacts seen in other heavy chalcogen heterocycles.³⁷ As described below, the four-center selenium clusters in 2a and 4a play a major role in increasing intermo-

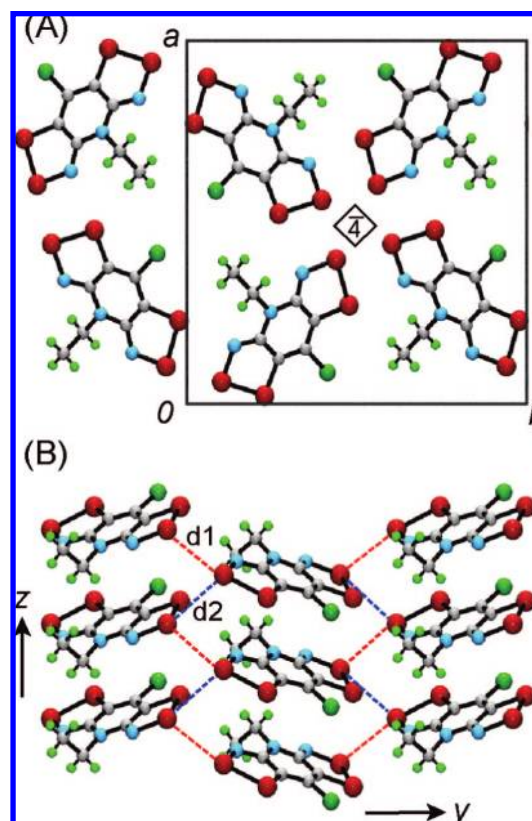


Figure 3. Crystal packing of 4a, viewed along the *z* (A) and *x* (B) directions.

lecular overlap and hence bandwidth. They also give rise to interesting magnetic properties.

Band Electronic Structures. In order to compare the extent of intermolecular electronic interactions in the four isostructural radicals 1a–4a we performed a series of EHT band structure calculations. The results must be viewed with caution, as the tight-binding model is inadequate for strongly correlated systems such as these. Nonetheless, within a closely related series of

(35) Bondi, A. *J. Phys. Chem.* **1964**, *68*, 441.

(36) This trend is replicated, but with closer contacts, at 100 K. For numerical details, see the Supporting Information.

(37) (a) Cozzolino, A. F.; Britten, J. F.; Vargas-Baca, I. *Cryst. Growth Des.* **2006**, *6*, 181. (b) Cozzolino, A. F.; Vargas-Baca, I.; Mansour, S.; Mahmoudkhani, A. H. *J. Am. Chem. Soc.* **2005**, *127*, 3184.

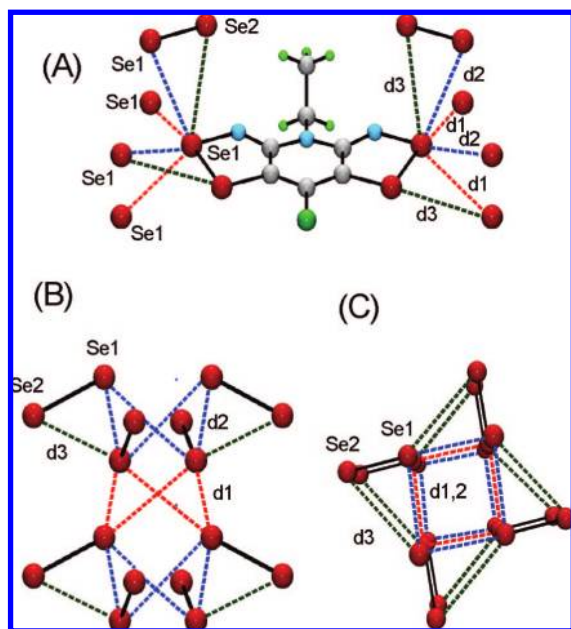


Figure 4. Intermolecular Se–Se' contacts d1–d3 to a single molecule of **4a** (A), and about the $\bar{4}$ centers, viewed perpendicular (B) and parallel (C) to the z direction.

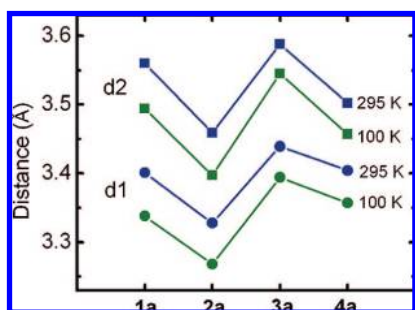


Figure 5. Variations in intermolecular E_2 – E_2' contacts d1 and d2 in **1a**–**4a**.

structures, as in the present case, the EHT method gives a qualitative insight into trends in orbital interactions, and hence bandwidth W , estimated here in terms of the energetic spread (dispersion) of the crystal orbitals (COs) under consideration. The results are summarized in Figure 6, which shows the dispersion of the COs arising from the four SOMOs in the respective unit cells, plotted along the reciprocal space direction $\Gamma(0, 0, 0)$ to $Z(0, 0, 1/2)$. By virtue of the tetragonal symmetry, CO trends along this reciprocal space vector can be associated precisely with orbital interactions along the stacking axis in real space. The tetragonal symmetry also leads to the degeneracy (coincidence) of two of the COs, and in the case of **2a** and **4a** there is an intruder orbital that falls in the same energy range.

From the spread of the dispersion curves across the series **1a**–**4a** it is readily apparent that the four compounds can be separated into two pairs, that is, those with sulfur (**1a/3a**) and those with selenium (**2a/4a**) in the E_2 -position. The increase in bandwidth between the two groups, from W near 0.5 eV to near 1.0 eV (Table 3), is quite dramatic, the latter values being significantly larger than in any slipped π -stack thiazyl or selenazyl radical we have ever seen. The increased CO dispersion which leads to this enhancement in W can, we believe, be attributed to the much tighter d1 and d2 contacts (Table 2 and Figure 5) about the $\bar{4}$ centers in **2a/4a**. Similarly,

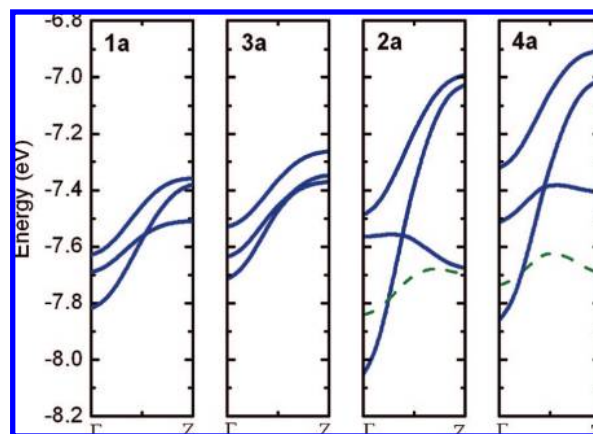


Figure 6. CO dispersion curves from $\Gamma(0, 0, 0)$ to $Z(0, 0, 1/2)$. Dashed green lines are intruder bands.

Table 3. Bandwidth, Conductivity, and Magnetic^a Parameters

	1a	2a	3a	4a
W (eV)	0.46 ^b	1.06	0.45	0.95
$\sigma(300\text{ K})$ (S cm^{-1})	3.2×10^{-6}	1.0×10^{-4}	2.2×10^{-5}	3.0×10^{-4}
E_{act} (eV)	0.43 ^b	0.27 ^c	0.31	0.19
C (emu K mol^{-1})	0.373 ^c	0.369	0.396	0.392
θ (K)	3.6 ^c	20.3	−2.3	22.9
T_c (K)	—	12.8	14	17.0
M_{sat} ($N\beta$) at 2 K	—	1.00	—	1.03
M_{rem} ($N\beta$) at 2 K	—	0.41	0.15×10^{-3}	0.43
H_c (Oe) at 2 K	—	250	66	1370

^a Data for **2a**–**4a** from samples prepared using TMPDA as reducing agent. ^b Data from ref 20a. ^c Data from ref 30.

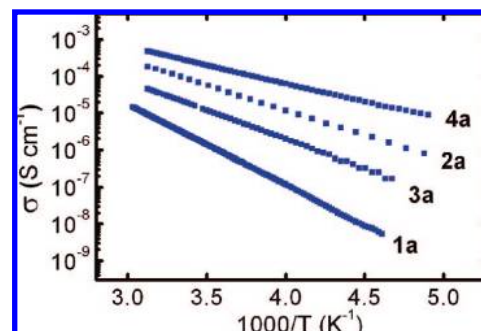


Figure 7. Log σ versus $1/T$ plots for **1a**–**4a**. Derived activation energies are in Table 3.

the slight decrease in bandwidth within the two pairs **1a/3a** and **2a/4a** can be related to the slight expansion in the contacts d1 and d2 occasioned by the replacement of sulfur by selenium in the E_1 position.

Conductivity Measurements. The results of the band structure calculations described above, especially the large bandwidths estimated for **2a** and **4a**, led us to anticipate an increased conductivity in these systems. Variable temperature, four-probe pressed pellet conductivity measurements on the four compounds confirmed these expectations. The results are presented in Figure 7 in the form of log plots of σ versus $1/T$. Despite the apparently large bandwidths, which for **2a** and **4a** are energetically comparable to U (arbitrarily estimated as $U \sim E_{\text{cell}}$), the materials are not metallic. Instead, the conductivity remains activated. There is, nonetheless, a satisfying correlation between the estimated (EHT) bandwidth, the observed conductivity and the derived thermal activation energy E_{act} (Table 3). Over the

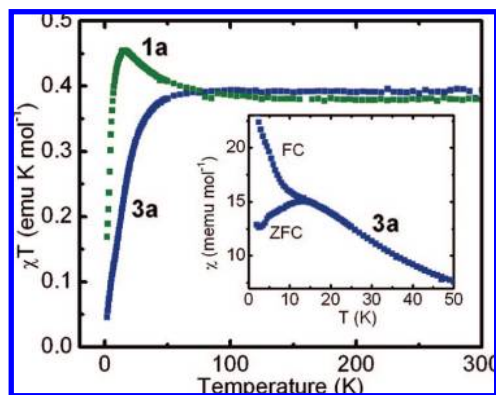


Figure 8. Plots of χT (field-cooled) versus temperature for **1a** and **3a** at 100 Oe. The insert shows ZFC-FC plots of χ versus T for **3a** at 100 Oe.

complete series, $\sigma(300\text{ K})$ increases by 2 orders of magnitude and E_{act} decreases with increasing selenium content from a maximum of 0.43 eV in **1a** to 0.19 eV in **4a**. Within the mixed S/Se systems **2a** and **3a**, the former has the higher conductivity and lower activation energy, in accord with the tighter d1,2 contacts and the resulting improvement in W .

Magnetic Measurements. Magnetic susceptibility measurements have been performed on **1a–4a** over the temperature range 2–300 K. At temperatures above 50 K, the static susceptibility χ (corrected for diamagnetic contributions)³⁸ of all four compounds follows paramagnetic behavior; values of C and θ derived from Curie–Weiss fits to the high temperature data are listed in Table 3. Below 50 K, however, there are some dramatic changes. For presentation and discussion purposes, results on the four compounds can be separated into two groups, that is, **1a** and **3a**, which contain sulfur in the E_2 position, and **2a** and **4a**, which have selenium at this site.

Figure 8 shows plots of the function χT versus T for the first group (**1a**, **3a**), measured in field-cooled mode at a field strength $H = 100$ Oe. In accord with its small positive θ -value, χT for **1a** rises slowly upon cooling from room temperature, indicative of weak local ferromagnetic interactions. It reaches a maximum ($0.46\text{ emu K mol}^{-1}$) at about 15 K and then drops rapidly as a result of weaker antiferromagnetic effects. Compound **3a** has a small but negative θ -value, indicative of weak antiferromagnetic coupling, and accordingly χT is seen to decrease rapidly at lower temperatures. Careful examination of the data below 20 K suggested a slight discontinuity, which became more apparent in a χ versus T plot. We therefore performed a series of zero-field-cooled (ZFC) and field-cooled (FC) experiments at different fields. The ZFC and FC curves of χ versus T are virtually coincident at 10 kOe, but when the field is reduced to 100 Oe, there is a separation in the two plots (Figure 8 insert), with a bifurcation or blocking temperature of 14 K. We have seen similar behavior for **3** (and **4**) with $R_1 = \text{Et}$, $R_2 = \text{H}$,²⁹ and, as for those systems, we believe the results here are a manifestation of a phase transition to a spin-canted antiferromagnetic state.

Further evidence in favor of this interpretation is provided by a measurement of the field-independent or spontaneous magnetization M_{sp} as a function of temperature. As shown in Figure 9, M_{sp} decays rapidly, approaching a plateau near zero at about $T = 14$ K, in accord with the blocking temperature noted in the ZFC-FC experiment. When extrapolated to $T = 0$ K, M_{sp} reaches a value of $0.18\text{ mN}\beta$, which can be used to

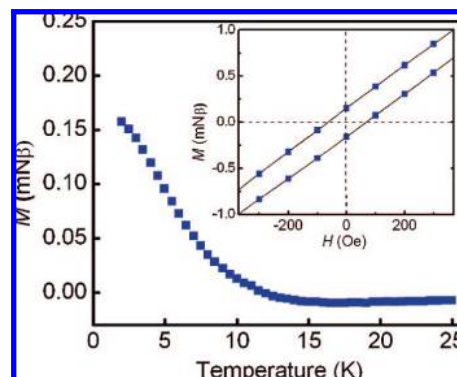


Figure 9. Field independent magnetization versus temperature for **3a**. The insert shows M vs H at 2 K.

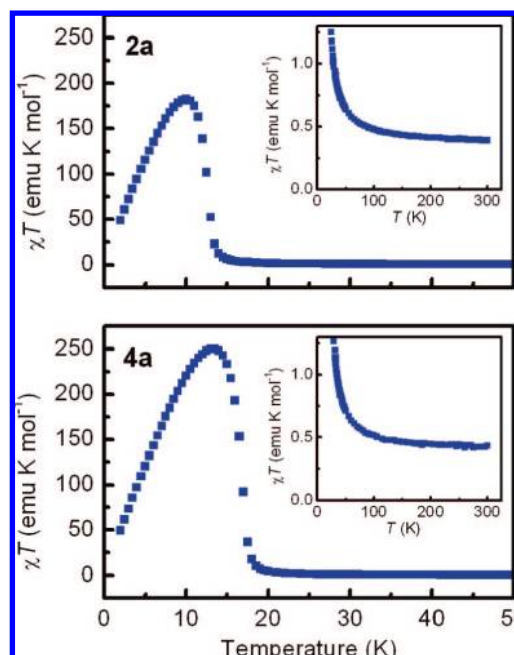


Figure 10. Plots of χT (field-cooled) versus temperature for **2a** and **4a** at 100 Oe. The inserts show an expansion of the high T region.

estimate a spin canting angle $\phi = 0.010^\circ$ by using the formula $\phi = \sin^{-1}(M_{\text{sp}}/M_{\text{sat}})$, where M_{sat} is approximated at $1\text{ N}\beta$, that is, the saturation value ($M_{\text{sat}} = gSN\beta$) of magnetization for a ferromagnetic material with $S = 1/2$ and $g = 2$. Magnetization experiments at 2 K as a function of field ($H = 0$ to 50 kOe) reveal a very weak, linear response with increasing field. The magnetization is slightly hysteretic (Figure 9 insert), as expected, giving rise to a coercive field $H_c = 66$ Oe (at 2 K) and remanent magnetization M_{rem} of $0.15\text{ mN}\beta$.

Plots of the product χT (field cooled) versus temperature for **2a** and **4a** at a field of $H = 100$ Oe (Figure 10) confirm that both compounds behave as paramagnets between 50 and 300 K, with $\chi T(300\text{ K})$ values of $0.392\text{ emu K mol}^{-1}$ (**2a**) and $0.432\text{ emu K mol}^{-1}$ (**4a**). Curie–Weiss fits to the data afford Curie constants C of $0.369\text{ emu K mol}^{-1}$ and $0.392\text{ emu K mol}^{-1}$, respectively, that is, near the value expected ($0.375\text{ emu K mol}^{-1}$) for an $S = 1/2$ system with g nominally equal to 2. The large positive Weiss constants of 20.3 K (**2a**) and 22.9 K (**4a**) herald strong local ferromagnetic exchange interactions. Upon cooling both compounds, there is a slow rise in χT , in keeping with the positive θ -values. A dramatic surge takes place just below 15 K for **2a** and 20 K for **4a**, with χT reaching a

(38) Carlin, R. L. *Magnetochemistry*; Springer-Verlag: New York, 1986.

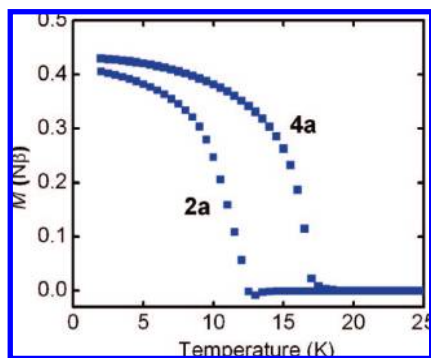


Figure 11. Field independent magnetization as a function of temperature for **2a** and **4a**.

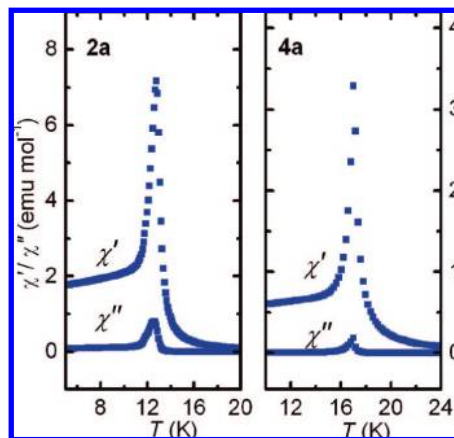


Figure 12. In-phase χ' and out-of-phase χ'' AC magnetic susceptibility (at 1 KHz) of **2a** and **4a** as a function of temperature.

maximum value of $182 \text{ emu K mol}^{-1}$ at 10 K for **2a** and of $244 \text{ emu K mol}^{-1}$ at 14 K for **4a**. This response is consistent with a phase transition to a ferromagnetically ordered state. At temperatures below these maxima there is a steady drop-off in χT for both compounds, as would be expected from low temperature magnetization saturation.

Measurements of the field independent magnetization M_{sp} of **2a** and **4a** provided further evidence for the existence of a ferromagnetically ordered state and also afforded a more accurate assessment of the ordering temperatures. As illustrated in Figure 11, M_{sp} is strongly temperature dependent for both compounds, decaying to zero near 12.5 and 17 K respectively, in accord with the point of maximum slope in the χT versus T plots described above. Back-extrapolation to $T = 0 \text{ K}$ afforded values of M_{sp} , the spontaneous magnetization at 0 K near $0.41 N\beta$ (**2a**) and $0.43 N\beta$ (**4a**), that is, three orders of magnitude greater than that seen for the spin-canted antiferromagnet **3a**. Variable temperature AC susceptibility measurements at different frequencies on **2a** and **4a** allowed us to pinpoint the ordering temperatures T_c of the two compounds. As shown in Figure 12, both radicals show sharp, well-defined maxima in the real (in-phase) χ' and imaginary (out-of-phase) χ'' components at 12.8 and 17.0 K, respectively. The invariance of T_c with changes in the cycling frequency (from 50 Hz to 5 kHz) establishes that these materials are not spin glasses.

Magnetization experiments as a function of field have also been performed on **2a** and **4a**. In both cases M rises sharply with H , reaching (at 2 K) a maximum at $H = 10 \text{ kOe}$, after which there is no further change in M with H (up to 55 kOe). The corresponding saturation magnetization values M_{sat} are 1.00

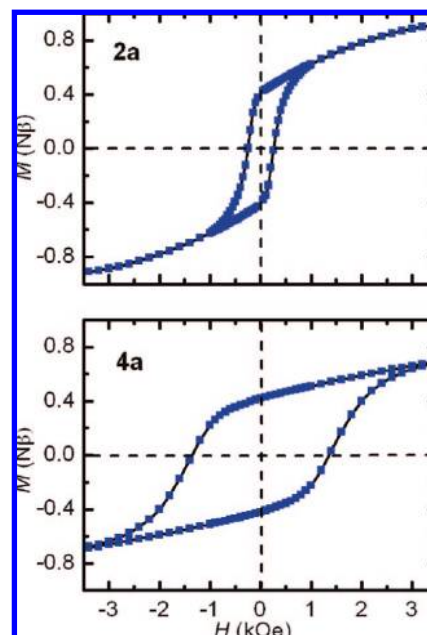


Figure 13. Magnetization of **2a** and **4a** as a function of magnetic field at 2 K.

$N\beta$ for **2a** and $1.03 N\beta$ for **4a**.³⁹ Reversal and cycling of the field sweep leads to hysteresis in the magnetization, the magnitude of which increases with increasing selenium content. Plots of M versus H , from measurements taken at 2 K on samples of the two compounds are shown in Figure 13. While the remanent magnetization M_{rem} of the two compounds is virtually the same, the coercive field H_c of **4a** (1370 Oe) is significantly greater than that found for **2a** (250 Oe).

Discussion

Our long-standing interest in the use of heterocyclic thiazyl radicals as building blocks for single component molecular conductors has been predicated on the idea that intermolecular overlap and hence bandwidth can be enhanced by the presence of a spatially extensive heteroatom.¹⁵ However, these materials suffered from (i) a propensity to dimerize and (ii) high on-site Coulomb repulsion barriers. With the development of resonance-stabilized systems such as **1a** these two problems were partly alleviated, but loss in bandwidth arising from π -stack slippage undermined attempts to achieve major improvements in conductivity.¹⁹ The incorporation of selenium to afford the series of S/Se-based materials **1a–4a** was driven by the belief that the heavier heteroatom would provide stronger intermolecular interactions and hence increased bandwidth. This approach had been explored in earlier generations of neutral radical conductors but had failed because of the seemingly inevitable tendency of the ensuing selenium-based radicals to associate in the solid state. The results on **1a–4a** demonstrate, at several levels, that replacement of sulfur by selenium works. We have shown, for the first time, that spin-pairing dimerization can be avoided across an entire series of mixed S/Se-based radicals. We have also achieved an isomorphous mapping across all four compounds, thereby allowing a detailed correlation of structure and transport properties. From a structural perspective, the major

(39) Spin-orbit effects raise the isotropic g -values of **2a** and **4a** (Table 1) above the free-electron mark of 2.0023, as a result of which the observation of $M_{\text{sat}} (= gS/N\beta)$ slightly greater than $1.0 N\beta$ for **4a** is not unexpected.

difference within the family **1a–4a** is the proximity of chalcogens about the 4 centers. The tightness of the d1 and d2 contacts when selenium occupies the E₂-position, that is, in **2a** and **4a**, leads to increased bandwidth in these compounds and a concomitant improvement in their conductivity relative to **1a** and **3a**. While the conductivity remains activated across the series, thermal activation energies are markedly reduced by heavy atom incorporation, especially so in **2a** and **4a**.

The magnetic properties of the selenium-based radicals described here can also be related, at least phenomenologically, to the presence of the heavy heteroatom. Almost all previous work on radical-based magnetic materials has focused on the use of light heteroatom (N, O) radicals. This approach has yielded a few magnetically ordered materials,⁸ but the Curie temperatures and coercive fields have always been low.⁹ The discovery of ordering, albeit spin-canted antiferromagnetism, in a dithiadiazolyl at 36 K¹⁰ represented a major step forward, partly for the increase in T_c , but more importantly as a proof of the concept that heavier heteroatoms, that is, sulfur, could afford stronger magnetic exchange interactions. Subsequent work has demonstrated ferromagnetic ordering (at 1.3 K) in a dithiadiazolyl,^{8d} but progress with these systems has been limited because the steric protection needed to avoid dimerization also reduces magnetic exchange via direct through-space interactions. Attempted extension of the heavy atom logic, by replacing sulfur in a sterically protected dithiadiazolyl radical with selenium, led to dimerization.⁴⁰

With the development of highly delocalized selenium-based radicals of the general type **2**, **3**, and **4**, in which association can be suppressed without the need for steric bulk, the door is opened to the pursuit of other⁴¹ heavy atom radicals capable of strong through-space magnetic interactions, be they ferromagnetic or antiferromagnetic. The variations in behavior along the series of compounds **2a**, **3a**, and **4a** attest to the critical importance of the location of the heavy atom on the sign of exchange coupling. Thus, only when selenium atoms are directly in contact about the 4 centers, as in **2a** and **4a**, is ferromagnetic ordering observed. In **3a**, the ordering is antiferromagnetic, although there is sufficient magnetic anisotropy, arising from spin–orbit contributions⁴² from selenium and/or the polar space group, to afford some spin canting.

While the ordering temperatures for **2a** and **4a** are no match for conventional inorganic ferromagnetic materials, they are an order of magnitude higher than those seen in light heteroatom ferromagnetic radicals. Indeed they are comparable to, and in one case (**4a**) greater than, the highest T_c values seen in nonmetal CT ferromagnets, that is, in materials such as TDAE·C₆₀ ($T_c = 16.1$ K)⁴³ or [BBDTA][GaCl₄] ($T_c = 8$ K).⁴⁴ Perhaps more striking than the ordering temperatures are the coercive fields observed for **2a** and **4a**, which are at least two orders of magnitude larger than those seen in light atom ferromagnets. While the origin of the magnetic response in these materials is far from understood, the T/θ ratios of 0.63 for **2a** and 0.74 for **4a** point to a significant degree of magnetic anisotropy, as might be expected from the crystal symmetry.³⁸ The appearance of

the hysteresis loops, with $M_{\text{rem}} \sim 1/2 M_{\text{sat}}$, is also broadly consistent with that expected for a highly anisotropic uniaxial system.⁴⁵

Presentation of the magnetic measurements for **2a** and **4a** would not be complete without a discussion of the dependence of the magnetic response of the materials on the nature of reducing agent used to generate them. As indicated in the synthesis section, the magnetic parameters reported here (listed in Table 3) refer to samples prepared using TMPDA as reducing agent. In contrast, the magnetic data described in our initial report on **2a** were obtained from samples prepared using TDAE. While the latter reagent afforded material that was analytically pure, its strong reducing properties led to more rapid nucleation and precipitation of the radicals. The resulting crystallites were smaller and, more importantly, also contained a greater number of structural defects which, in turn, affected the magnetic response. Thus, the slightly lower values for C (0.349 emu mol⁻¹) and M_{sat} (0.95 N β) for **2a** cited in our initial report³⁰ can be ascribed to the presence of a low concentration of diamagnetic dimers. In order to test this interpretation, we explored the response of **4a** to changes in reductant and to our satisfaction found the same dependency. A sample of **4a** prepared using TDAE provided lower C (0.340 emu mol⁻¹) and M_{sat} (0.94 N β) values.

We also point out that the coercive field H_c for **2a** listed in Table 3 is smaller than that reported (590 Oe) in our initial communication,³⁰ where TDAE was used to generate the radical. A similar trend has been found for **4a**; the H_c value (at 2 K) of a sample prepared using TDAE was 2030 Oe, that is, larger than that of the TMPDA-produced material (1370 Oe).⁴⁶ The increased coercivity observed for the TDAE-produced samples is not unexpected. The defects that lead to a slight suppression in C and M_{sat} may also serve to pin domain boundaries and inhibit the reversal of magnetization, thereby increasing H_c .⁴⁵

Summary and Conclusions

For many years the development of molecular conductors and magnetic materials based on neutral radicals has evolved along separate, nonconverging paths. Work on conductors has focused on (i) radicals which possess extensive spin delocalization, to lower the onsite Coulomb barrier U , and (ii) the incorporation of heavy heteroatoms (sulfur) to increase intermolecular overlap and hence bandwidth W . By contrast most magnetic materials have been built using light heteroatom radicals, in which spin density is more localized. In addition, steric bulk is often employed to suppress dimerization. This combination of spin localization, which increases U , and molecular bulk, which decreases W , militates against the use of these materials as molecular conductors.

Because of these apparently conflicting design criteria, the possibility that the unpaired electrons in molecular radicals might serve simultaneously as carriers of charge and spin has received limited consideration.^{47,48} The resonance-stabilized selenazyl radicals reported here demonstrate that multifunctionality, that is, bulk ferromagnetism and activated conductivity, can be

(40) Feeder, N.; Less, R. J.; Rawson, J. M.; Oliete, P.; Palacio, F. *Chem. Commun.* **2000**, 2449.

(41) García, F.; Less, R. J.; Naseri, V.; McPartlin, M.; Rawson, J. M.; Wright, D. S. *Angew. Chem., Int. Ed.* **2007**, *46*, 7827.

(42) (a) Dzyaloshinsky, I. *J. Phys. Solids* **1958**, *4*, 241. (b) Moriya, T. *Phys. Rev.* **1960**, *120*, 91.

(43) Allemand, P. M.; Khemani, K. C.; Koch, A.; Wudl, F.; Holczer, K.; Donovan, S.; Gruner, G.; Thompson, J. D. *Science* **1991**, *253*, 301.

(44) Fujita, W.; Awaga, K. *Chem. Phys. Lett.* **2004**, *388*, 186.

(45) (a) Chikazume, S. *Physics of Magnetism*; John-Wiley: New York, 1964. (b) Bertotti, G. *Hysteresis in Magnetism*; Academic Press: New York, 1998.

(46) Details of these measurements are provided in the Supporting Information.

(47) Dooley, B. M.; Bowles, S. E.; Storr, T.; Frank, N. L. *Org. Lett.* **2007**, *9*, 4781.

(48) (a) Prigodin, V. N.; Raju, N. P.; Pokhondnya, K. I.; Miller, J. S.; Epstein, A. J. *Adv. Mater.* **2002**, *14*, 1230. (b) Blundell, S. J.; Pratt, F. L. *J. Phys.: Condens. Matter* **2004**, *16*, R771.

generated using a single component molecular radical. While the T_c values of the present materials are still too low to allow measurements of conductivity in the ferromagnetic regime, it is possible that chemical and structural modifications of the present systems may lead to improvements in T_c and/or conductivity, so that field-dependent conductivity can be probed. The application of physical pressure should also increase both conductivity^{27b} and T_c ⁴⁹ and may even afford materials displaying itinerant ferromagnetism.

The importance of magnetic purity, that is, the need to optimize the reduction of the cations to the radicals so as to minimize structural defects, cannot be overstated. While such defects lead to relatively small departures in C and M_{sat} values from ideal behavior, the variations in H_c are much larger. Further studies of the dependence of coercivity on sample preparation, that is, the effect of grain size and crystal growth rate, are ongoing.

Experimental Section

General Procedures and Starting Materials. The reagents selenium dioxide, thionyl chloride, Proton Sponge, sodium borohydride, methyl iodide, ethyl triflate, gallium trichloride, tetra-*n*-butylammonium triflate, octamethylferrocene (OMFc), tetrakis(dimethylamino)ethylene (TDAE), and *N,N,N',N'*-tetramethyl-*p*-phenylenediamine (TMPDA) were obtained commercially. Compound [1a][OTf],^{20a,c} iodobenzene dichloride,⁵⁰ and potassium selenocyanate⁵¹ were prepared according to literature methods. OMFc was purified by sublimation in vacuo and recrystallization from acetonitrile, TDAE was purified by double distillation in vacuo, and TMPDA was purified by sublimation in vacuo. The solvents acetonitrile (MeCN), dichloroethane (DCE), acetic acid (HOAc), dichloromethane (DCM), and tetrahydrofuran (THF) were of at least reagent grade. MeCN was dried by distillation from P₂O₅ and/or CaH₂, and both DCE and DCM by distillation from P₂O₅. All reactions were performed under an atmosphere of dry nitrogen. Melting points are uncorrected. Infrared spectra (Nujol mulls, KBr optics) were recorded on a Nicolet Avatar FTIR spectrometer at 2 cm⁻¹ resolution. ¹H spectra were run on a Bruker Avance 300 MHz NMR spectrometer, and low resolution ESI mass spectra were run on a Micromass Q-TOF Ultima Global LC/MS/MS system. Elemental analyses were performed by MHW Laboratories, Phoenix, AZ 85018.

Preparation of 8-Chloro-4-ethyl-4*H*-bis[1,2,3]thiaselenazolo[4,5-*b*:5',4'-*e*]pyridin-2-ium Triflate [2a][OTf]. Compound [1a][OTf] (0.884 g, 2.00 mmol) and finely ground selenium dioxide (0.666 g, 6.00 mmol) were added to a large glass pressure vessel along with 80 mL of MeCN, and the mixture stirred and heated in an oil bath at 110 °C for 48 h. Analysis of the mixture at this time by ESI mass spectrometry showed complete and specific formation of [2a]⁺. The flask was cooled to room temperature and the dark green solution filtered through a glass Büchner funnel to remove a small amount of black precipitate. The filtrate was concentrated to 30 mL and cooled to room temperature for 1 h and then at -20 °C for 2 h. Red crystals of [2a][OTf] (0.704 g, 1.31 mmol, 65%) were filtered off, washed with DCM, and dried in air. The product was double recrystallized from MeCN as red needles, mp 294–6 °C. IR: 2254 (w, MeCN), 1453 (m), 1435 (s), 1282 (s), 1245 (vs), 1184 (w), 1155 (s), 1073 (w), 1026 (s), 1004 (w), 757 (w), 742 (s), 720 (w), 636 (s), 598 (m), 533 (w), 516 (m), 476 (w) cm⁻¹. Samples for elemental analysis were heated overnight at 78 °C/10⁻² Torr

to remove the MeCN solvate. Anal. Calcd for C₈H₅ClF₃N₃O₃S₃Se₂: C, 17.87; H, 0.94; N, 7.81%. Found: C, 17.73; H, 0.87; N, 7.57%.

Preparation of 2,6-Diaminopyridine-3,5-bis(selenocyanate) 5. A solution of bromine (8.90 mL, 0.173 mol) in 100 mL of MeOH was added dropwise over a 1 h period to a cold (-78 °C) solution of potassium selenocyanate (50.0 g, 0.347 mol) in 200 mL of MeOH. A solution of 2,6-diaminopyridine (9.45 g, 0.0866 mol) in 150 mL of MeOH was then added dropwise over 90 min, and the subsequent orange mixture was stirred for 1 h at -78 °C. The mixture was poured onto 1.5 L ice/water and left to stand at room temperature for 20 h. The resulting gray solid was filtered off and warmed in 1.5 L 10% aq HCl for 2 h. Upon filtration, the yellow filtrate was cooled to 0 °C and then made basic (pH 8–9) with aqueous ammonia. After 2 h, the yellow microcrystalline precipitate was collected by filtration and washed with water. The acid/base extraction was repeated several times to afford an overall yield for 2,6-diaminopyridine-3,5-bis(selenocyanate) **5** of 19.6 g (0.0619 mol, 71%); mp >200 °C dec IR: 3490 (m), 3427 (s), 3382 (s), 3325 (w), 3151 (m, br), 3047 (w), 2145 (s), 1655 (s), 1627 (s), 1603 (s), 1555 (m), 1532 (s), 1460 (s), 1377 (s), 1311 (vw), 1260 (w), 1077 (vw), 1022 (vw), 952 (w), 800 (vw), 755 (m), 722 (w), 619 (vw), 566 (vw), 502 (w), 458 (w) cm⁻¹. Anal. Calcd for C₇H₅N₅Se₂: C, 26.52; H, 1.59; N, 22.09%. Found: C, 26.70; H, 1.39; N, 22.06%.

Preparation of 2,6-Diamino-3,5-bis(selenomethyl)pyridine 6. A slurry of **5** (13.0 g, 0.0410 mol) in 225 mL of MeOH was cooled to 0 °C, and sodium borohydride (5.10 g, 0.135 mol) was added slowly to give a clear yellow solution. After 30 min, methyl iodide (8.40 mL, 0.135 mol) was added and the reaction mixture was stirred for 1 h at 0 °C before being poured onto 1 L ice/water. After 2 h the yellow product was filtered off and washed with water, yield 11.1 g (0.0419 mol, 92%). Recrystallization from 60 mL of ethyl acetate afforded colorless needles of **6**; yield 9.89 g (0.0335 mol, 89% from crude); mp 120–122 °C. IR: 3408 (m), 3282 (m, br), 3177 (vw), 1599 (s), 1544 (s), 1463 (vs), 1425 (vs), 1377 (vs), 1300 (w), 1266 (m), 1237 (w), 1153 (w), 1031 (w), 937 (m), 907 (s), 765 (s), 720 (m), 688 (vw), 634 (m, br), 584 (m), 449 (m) cm⁻¹. ¹H NMR (δ, CDCl₃): 7.81 (s, 1H, aromatic), 5.01 (s, 4H, amino), 2.10 (s, 6H, methyl). Anal. Calcd for C₇H₁₁N₃Se₂: C, 28.49; H, 3.76; N, 14.24%. Found: C, 28.69; H, 3.87; N, 14.40%.

Preparation of 4*H*-Bis[1,2,3]selenathiazolo[4,5-*b*:5',4'-*e*]pyridin-2-ium Chloride, [3][Cl] (R₁ = R₂ = H). Triethylamine (21.4 mL, 0.154 mol) was added to a slurry of **6** (11.3 g, 0.0382 mol) in 500 mL of MeCN, and the mixture was cooled to 0 °C. A solution of thionyl chloride (16.8 mL, 0.230 mol) in 100 mL of MeCN was then added over a period of 90 min to afford a dark brown precipitate. The slurry mixture was stirred for 16 h at room temperature, during which time the precipitate slowly turned black. This black precipitate of [3][Cl] (R₁ = R₂ = H) was filtered off and washed 3 × 200 mL of MeCN and 2 × 200 mL of DCM; yield 11.2 g (0.0309 mol, 81%). IR: 1344 (s), 1261 (w), 1073 (w), 1031 (s), 885 (m), 806 (m), 735 (s), 711 (m), 691 (m), 609 (s), 496 (w), 446 (m) cm⁻¹.

Preparation of 4*H*-Bis[1,2,3]selenathiazolo[4,5-*b*:5',4'-*e*]pyridin-2-ium Triflate, [3][OTf] (R₁ = R₂ = H). Gallium trichloride (6.25 g, 0.0355 mol) was added to a slurry of [3][Cl] (R₁ = R₂ = H) (11.2 g, 0.0309 mol) in 400 mL of MeCN. After 30 min, the solution was filtered through a fine (E porosity) frit, and the solvent was removed by flash distillation. The copper-red residue of crude [3][GaCl₄] (R₁ = R₂ = H) was tritreated with 200 mL of HOAc and filtered off, washed with 4 × 150 mL of HOAc and 2 × 100 mL of DCM; yield 12.2 g (0.0226 mol, 73%). IR: 1497 (w), 1347 (s), 1262 (w), 1029 (s), 899 (m), 867 (w), 838 (w), 817 (m), 729 (s), 687 (m), 615 (s), 445 (w) cm⁻¹. Crude [3][GaCl₄] (R₁ = R₂ = H) (12.2 g, 0.0226 mol) was dissolved in 100 mL of hot anhydrous THF and the resulting mixture hot filtered. Tetrabutylammonium triflate (10.7 g, 0.0272 mol) dissolved in 60 mL of DCE was added to the filtrate. After 1 h, the resulting red precipitate of [3][OTf] (R₁ = R₂ = H) was collected by filtration and washed with 4 × 60 mL of DCE, yield 6.46 g (0.0136 mol, 60%); mp >227 °C dec IR:

- (49) (a) Mito, M.; Kawae, T.; Takeda, K.; Takagi, S.; Matsushita, Y.; Deguchi, H.; Rawson, J. M.; Palacio, F. *Polyhedron* **2001**, *20*, 1509. (b) Mito, M.; Fujino, M.; Deguchi, H.; Takagi, S.; Fujita, W.; Awaga, K. *Polyhedron* **2005**, *24*, 2501.
(50) Brauer, G. *Handbook of Preparative Inorganic Chemistry*; Academic: New York, 1963; Vol. 1, p 423.
(51) Waitkins, G. R.; Shutt, R.; McReynolds, J. P.; McFadden, R. L. *Inorg. Synth.* **1946**, *2*, 186.

3197 (w), 1328 (s), 1257 (s), 1230 (s), 1166 (m), 1022 (s), 895 (w), 812 (m), 760 (w), 731 (m), 715 (s), 689 (m), 638 (m), 607 (s), 577 (w), 572 (w), 519 (w), 511 (m), 446 (s) cm^{-1} . Anal. Calcd for $\text{C}_6\text{H}_2\text{F}_3\text{N}_3\text{O}_3\text{S}_3\text{Se}_2$: C, 15.16; H, 0.42; N, 8.84%. Found: C, 15.56; H, 0.50; N, 9.08%.

Preparation of Bis[1,2,3]selenathiazolo[4,5-*b*:5',4'-*e*]pyridin-2-ium-4-ide, 7. Proton sponge (3.51 g, 0.0164 mol) was added as a dry solid to a slurry of [3][OTf] ($\text{R}_1 = \text{R}_2 = \text{H}$) (6.46 g, 0.0136 mol) in 250 mL of MeCN. After 16 h the green precipitate of 7 was filtered off and washed with 4×100 mL of MeCN; yield 4.49 g (0.0138 mol, 99%). IR: 1414 (m), 1345 (m), 1257 (w), 1047 (w), 1018 (m), 900 (s), 814 (w), 729 (m), 720 (s), 674 (w), 619 (m) cm^{-1} .

Preparation of 4-Ethyl-4*H*-bis[1,2,3]selenathiazolo[4,5-*b*:5',4'-*e*]pyridin-2-ium Triflate, [3][OTf] ($\text{R}_1 = \text{Et}$, $\text{R}_2 = \text{H}$). Ethyl triflate (4.5 mL, 0.0348 mol) was added to a solution of Proton Sponge (1.48 g, 6.89 mmol) in 200 mL of DCE. Compound 7 (4.49 g, 0.0138 mol) was added and the mixture stirred for 3–4 days. The fine red precipitate of crude [3][OTf] ($\text{R}_1 = \text{Et}$, $\text{R}_2 = \text{H}$) was filtered off, washed with 3×80 mL of DCE, and dried in vacuo; yield 5.81 g (0.0115 mol, 84%). The product was recrystallized from MeCN and HOAc and isolated as lustrous red needles; mp >235 °C dec IR: 3088 (w), 1353 (s), 1263 (s), 1250 (m), 1238 (m), 1223 (m), 1175 (m), 1156 (m), 1146 (m), 1085 (w), 1035 (w), 1027 (m), 989 (w), 904 (w), 830 (m), 792 (s), 759 (w), 729 (s), 650 (m), 638 (s), 574 (m), 516 (s), 465 (m) cm^{-1} . Anal. Calcd for $\text{C}_8\text{H}_6\text{F}_3\text{N}_3\text{O}_3\text{S}_3\text{Se}_2$: C, 19.09; H, 1.20; N, 8.35%. Found: C, 19.06; H, 1.26; N, 8.42%.

Preparation of 8-Chloro-4-ethyl-4*H*-bis[1,2,3]selenathiazolo[4,5-*b*:5',4'-*e*]pyridin-2-ium Triflate, [3a][OTf]. Freshly prepared iodobenzene dichloride (1.42 g, 5.15 mmol) was added to a slurry of [3][OTf] ($\text{R}_1 = \text{Et}$, $\text{R}_2 = \text{H}$) (2.36 g, 4.69 mmol) in 300 mL of MeCN and the reaction mixture heated to a gentle reflux for 1 h before being filtered hot to remove any insoluble material. The filtrate was concentrated to 100 mL and allowed to stand at room temperature for 16 h. Red crystals of crude [3a][OTf] were filtered off and washed with DCM; yield 1.77 g (3.29 mmol, 70%). The product was purified by recrystallization from MeCN and HOAc to afford lustrous red needles; mp >270 °C dec IR: 1499 (m), 1446 (s), 1434 (s), 1356 (s), 1273 (m), 1242 (s), 1185 (m), 1169 (m), 1076 (m), 1027 (s), 997 (w), 881 (m), 841 (m), 810 (w), 790 (w), 655 (s), 637 (s), 597 (s), 573 (w), 551 (w), 517 (m) cm^{-1} . Anal. Calcd for $\text{C}_8\text{H}_5\text{ClF}_3\text{N}_3\text{O}_3\text{S}_3\text{Se}_2$: C, 17.87; H, 0.94; N, 7.81%. Found: C, 17.90; H, 1.04; N, 7.91%.

Preparation of 8-Chloro-4-ethyl-4*H*-bis[1,2,3]diselenazolo[4,5-*b*:5',4'-*e*]pyridin-2-ium Triflate, [4a][OTf]. Finely ground selenium dioxide (0.900 g, 8.11 mmol) was added to a hot solution of [3a][OTf] (1.31 g, 2.43 mmol) in 120 mL of HOAc. The mixture was heated at reflux for 90 min and then cooled slowly to room temperature. After 16 h, crude [4a][OTf] was filtered off and washed with DCM; yield 0.850 g (1.35 mmol, 55%). Dark purple needles were isolated by recrystallization from HOAc, mp >255 °C dec IR: 1417 (s), 1355 (s), 1280 (s), 1245 (s), 1224 (m), 1180 (w), 1156 (s), 1084 (w), 1062 (w), 1026 (s), 987 (w), 923 (w), 773 (w), 757 (m), 751 (w), 727 (m), 636 (s), 579 (s), 549 (m), 517 (s) cm^{-1} . Anal. Calcd for $\text{C}_8\text{H}_5\text{ClF}_3\text{N}_3\text{O}_3\text{S}_2\text{Se}_4$: C, 15.22; H, 0.80; N, 6.65%. Found: C, 15.40; H, 0.68; N, 6.51%.

Preparation of Radicals: Method 1.

Bulk Material for Conductivity and Magnetic Measurements. Before use, all glassware was soaked overnight in dilute HNO_3 , washed with deionized water followed by distilled water, and finally oven-dried at 100 °C overnight. Magnetic stirbars were glass-covered. Degassed solutions (three freeze–pump–thaw cycles) of TMPDA (0.330–0.586 mmol) in 40–75 mL of MeCN and [2a–4a][OTf] (0.317–0.558 mmol) in 120–150 mL of MeCN were combined, and after 30 min the gold-brown precipitate of 2a–4a was filtered off and washed 4×20 mL of MeCN. **Method 2A. Diffusion H-cells for single crystal growth of 2a, 3a.** Degassed solutions (3 freeze–pump–thaw cycles) of OMFc (0.058 mmol) in 15 mL of MeCN and [2a, 3a][OTf] (0.055 mmol) in 15 mL of

MeCN were allowed to diffuse together slowly at room temperature over a period of 16 h. The solvent was decanted to leave metallic green/black needles of 2a, 3a suitable for X-ray work. **Method 2B. Electrocrystallization H-Cells for Single Crystal Growth of 4a.** The electrocrystallization work employed standard electrochemical H-cell techniques,⁵² with samples of [4a][OTf] (20 mg) dissolved under nitrogen in 20 mL of MeCN containing 0.008 M [*n*-Bu₄N][PF₆] as supporting electrolyte. Currents ranged from 5 to 10 μA , with growth periods of 2–4 days.

Analytical Data for Radicals. 2a. Yield 88% (Method 1), dec >120 °C. IR: 1442 (s), 1409 (w), 1324 (m), 1228 (s), 1172 (m), 1082 (m), 1065 (m), 914 (w), 840 (s), 729 (s), 719 (m), 694 (s), 580 (m), 534 (w), 459 (m) cm^{-1} . Anal. Calcd for $\text{C}_7\text{H}_5\text{ClN}_3\text{S}_2\text{Se}_2$: C, 21.63; H, 1.30; N, 10.81%. Found: C, 21.66; H, 1.26; N, 10.86%. **3a.** Yield 86% (Method 1), dec >120 °C. IR: 1485 (w), 1441 (s), 1416 (s), 1352 (w), 1328 (w), 1315 (m), 1217 (s), 1177 (m), 1079 (m), 1066 (w), 993 (m), 856 (m), 782 (s), 699 (s), 681 (s), 668 (w), 648 (s), 633 (s), 592 (s), 526 (m), 490 (m), 465 (s) cm^{-1} . Anal. Calcd for $\text{C}_7\text{H}_5\text{ClN}_3\text{S}_2\text{Se}_2$: C, 21.63; H, 1.30; N, 10.81%. Found: C, 21.49; H, 1.31; N, 10.60%. **4a.** Yield 85% (Method 1), dec >120 °C. IR: 1403 (w), 1316 (m), 1224 (s), 1167 (m), 1078 (w), 1058 (m), 988 (m), 812 (m), 689 (s), 573 (m), 559 (w), 535 (w), 432 (w) cm^{-1} . Anal. Calcd for $\text{C}_7\text{H}_5\text{ClN}_3\text{Se}_4$: C, 17.43; H, 1.04; N, 8.71%. Found: C, 17.17; H, 1.23; N, 8.66%.

Cyclic Voltammetry. Cyclic voltammetry was performed using a PINE Bipotentiostat, Model AFCCIBP1, with scan rates of 50–100 mV s^{-1} on solutions ($<10^{-3}$ M) of [1a–4a][OTf] in oxygen-free MeCN (dried by distillation from CaH_2) containing 0.1 M tetra-*n*-butylammonium hexafluorophosphate. Potentials were scanned with respect to the quasireference electrode in a single compartment cell-fitted with Pt electrodes and referenced to the F_2/Fc^+ couple of ferrocene at 0.38 V vs SCE.⁵³ The $E_{\text{pa}}-E_{\text{pc}}$ separation of the reversible couples was within 10% of that of the F_2/Fc^+ couple.

EPR Spectroscopy. The X-band EPR spectra of 1a–4a were recorded at ambient temperature using a Bruker EMX-200 spectrometer on samples of the radicals dissolved in degassed dichloromethane and/or toluene. Hyperfine coupling constants were obtained by spectral simulation using PEST Winsim⁵⁴ and Bruker WinEPR Simfonia.⁵⁵

X-ray Measurements. Needles of 1a–4a were glued to glass fibers with epoxy. X-ray data (at ambient temperature for 3a–4a and also at 100 K for 1a–4a) were collected using omega scans with a Bruker APEX I CCD detector on a D8 three-circle goniometer and Mo K_α ($\lambda = 0.71073$ Å) radiation. The data were scanned using Bruker's SMART program and integrated using Bruker's SAINT software.⁵⁶ The structures were solved by direct methods using SHELXS-90⁵⁷ and refined by least-squares methods on F^2 using SHELXL-97⁵⁸ incorporated in the SHELXTL⁵⁹ suite of programs.

Magnetic Susceptibility Measurements. DC magnetic susceptibility measurements were performed over the range 2–300 K on

- (52) (a) Ferraro, J. R.; Williams, J. M. *Introduction to Synthetic Electrical Conductors*; Academic: New York, 1987; p 25. (b) Stephens, D. A.; Rehan, A. E.; Compton, S. J.; Barkhau, R. A.; Williams, J. M. *Inorg. Synth.* **1986**, *24*, 135.
 (53) Boeré, R. T.; Moock, K. H.; Parvez, M. Z. *Anorg. Allg. Chem.* **1994**, *620*, 1589.
 (54) Duling, D. R. *J. Mag. Reson., Ser. B* **1994**, *104*, 105.
 (55) WinEPR Simfonia, version 1.25; Bruker Instruments, Inc., Billerica, MA, 1996.
 (56) SAINT, version 6.22; Bruker Advanced X-ray Solutions, Inc., Madison, WI, 2001.
 (57) Sheldrick, G. M. *Acta Crystallogr., Sect. A: Found. Crystallogr.* **1990**, *46*, 467.
 (58) Sheldrick, G. M. *SHELXL-97; Program for the Refinement of Crystal Structures*, University of Göttingen, Göttingen, Germany, 1997.
 (59) *SHELXTL, Version 6.12, Program Library for Structure Solution and Molecular Graphics*, Bruker Advanced X-ray Solutions, Inc., Madison, WI, 2001.

a Quantum Design MPMS SQUID magnetometer. AC susceptibility measurements were performed on an Oxford Instruments MagLab EXA.

Conductivity Measurements. Temperature dependent conductivity measurements were performed (in duplicate) on pressed pellet samples using a four-probe method. A homemade device was used to measure the voltage drop under dynamic vacuum. Silver paint was used to apply the electrical contacts.

Band Structure Calculations. Band electronic structure calculations were performed with the EHMACC suite of programs⁶⁰ using the Coulomb parameters of Baasch, Viste, and Gray⁶¹ and a quasisplit valence basis set adapted from Clementi and Roetti;⁶² numerical values are tabulated elsewhere.^{25a} The off-diagonal elements of the Hamiltonian matrix were calculated with the standard weighting formula.⁶³ Atomic positions were taken from the ambient temperature crystallographic data.

(60) EHMACC, Quantum Chemistry Program Exchange, program number 571, University of Indiana, Bloomington, IN.

(61) Basch, H.; Viste, A.; Gray, H. B. *Theor. Chim. Acta* **1965**, *3*, 458.

(62) Clementi, E.; Roetti, C. *At. Data. Nucl. Data Tables* **1974**, *14*, 177.

(63) Ammeter, J. H.; Bürgi, H. B.; Thibault, J. C.; Hoffmann, R. *J. Am. Chem. Soc.* **1978**, *100*, 3686.

Acknowledgment. This paper is dedicated to Professor Norman L. Paddock on the occasion of his 90th birthday. We thank the Natural Sciences and Engineering Research Council of Canada (NSERCC) for financial support. We also acknowledge the NSERCC for a Canada Graduate Scholarship to A. A. L., the Ontario Government for a Graduate Scholarship to C. M. R. and the Canada Council for a Killam Research Fellowship to R. T. O. We are indebted to Dr. Richard Smith for ESI-MS analyses.

Supporting Information Available: Complete authorship for ref 25b. Details of X-ray crystallographic data collection and structure refinement at ambient temperature and 100 K, tables of atomic coordinates, bond distances and angles, anisotropic thermal parameters, and hydrogen atom positions in CIF format. Details of magnetic measurements and reducing agents. This information is available free of charge via the Internet at <http://pubs.acs.org>.

JA801070D